Appl. Phys. A (2017) 123:209
DOI 10.1007/s00339-017-0834-4

Applied Physics A
Materials Science & Processing

Generation of ultra-small InN nanocrystals by pulsed laser ablation of suspension in organic solution

Canan Kurşungöz[1,2] · Elif Uzcengiz Şimşek[1,2] · Refik Tuzaklı[1] · Bülend Ortaç[1,2]

Received: 7 December 2016 / Accepted: 3 February 2017 / Published online: 2 March 2017

Abstract Nanostructures of InN have been extensively investigated since nano-size provides a number of advantages allowing applications in nanoscale electronic and optoelectronic devices. It is quite important to obtain pure InN nanocrystals (InN-NCs) to reveal the characteristic features, which gain interest in the literature. Here, we proposed a new approach for the synthesis of ultra-small hexagonal InN-NCs by using suspension of micron-sized InN powder in ethanol with pulsed laser ablation method. The liquid environment, laser energy and ablation time were optimized and a post-synthesis treatment, centrifugation, was performed to achieve InN-NCs with the smallest size. Besides, the micron-sized InN powder suspension, as a starting material, enabled us to obtain InN-NCs having diameters smaller than 5 nm. We also presented a detailed characterization of InN-NCs and demonstrated that the formation mechanism mainly depends on the fragmentation due to laser irradiation of the suspension.

1 Introduction

The promising optoelectronic properties of Group III nitrides (InN, GaN, AlN) led to an increasing attention due to their potential applications [1]. Among them, due to its smallest effective mass, high electron mobility, superior electron transport properties and direct band gap structure, InN is a promising candidate for high-speed optoelectronic devices, broad-spectrum solar cells, high electron mobility transistors, near infrared light emitting diodes (LEDs) and high-speed laser diodes [2–4]. Furthermore, its nontoxic nature and infrared emission properties enable InN to be used in biological and medical applications [5]. Besides these advantageous properties of InN material, its nanostructures have been widely studied due to their different characteristics depending on the dimensionality and size, which allow the applications in nanoscale electronic and optoelectronic devices [6, 7].

InN crystallizes in two different structures: stable hexagonal (wurtzite) structure and metastable cubic structure. When compared to hexagonal InN, cubic InN possesses smaller band gap and superior electronic properties due to its isotropic lattice and lower phonon scattering [8]. However, the production of cubic InN-NCs is quite a challenging process due to its thermodynamically unstable nature [9]. Previous studies showed a number of techniques viable for the synthesis of InN-NCs mainly having hexagonal structure. Ambient pressure and low-temperature liquid phase was proposed as a suitable method for the synthesis of nanoparticles having low decomposition temperatures. It was shown that wurtzite InN-NCs having 6.2 nm average diameter are successfully produced using this method. These colloidal wurtzite InN-NCs were post-treated with nitric acid to get rid of the metallic indium byproduct and finally InN nano-powder was obtained [10]. Moreover, activated reactive evaporation and nitrogen plasma annealing methods were proposed for the successful production of wurtzite InN-NCs and InN nanorods, respectively. It was suggested that the technique is applicable to produce InN-NCs by using low temperatures from indium nanostructures obtained by different techniques [11]. Xiao et al.

✉ Bülend Ortaç
ortac@unam.bilkent.edu.tr

[1] Materials Science and Nanotechnology Department, UNAM-National Nanotechnology Research Center, Bilkent University, 06800 Ankara, Turkey

[2] Institute of Materials Science and Nanotechnology, Bilkent University, 06800 Ankara, Turkey

demonstrated the synthesis of 10–30 nm InN-NCs from sulfide precursor using a novel thermal conversion method at low temperatures and suggested that this method can be applied for the production of all group III nitrides [12]. The synthesis of wurtzite InN nanobelts was also performed by using guided-stream thermal chemical vapor deposition (GSCVD) technique [13]. Qaeed et al. proposed a chemical synthesis method not requiring high temperatures for large-scale nanoparticle production. These InN-NCs were shown to be cubic in structure and to have a grain size between 11.4 and 21.4 nm [14]. On the other hand, rapid thermal ammonolysis was shown as a method for production of InN-NCs in hexagonal crystal structure [15]. Single-crystalline InN-NCs having an average diameter of 15 nm and hexagonal structure were successfully produced using vapor–liquid–solid process [16]. Furthermore, single-crystalline hexagonal structured InN-NCs having 9.8–36.0 nm grain size were obtained by the reaction of InI_3 and $NaNH_2$ in benzene-thermal system [17].

Pulsed laser ablation in liquid (PLAL) is a promising top-down approach for nanoparticle production and it allows production of wide variety of nanoparticles such as metal, metal oxide, nitride and semiconductor nanocrystals [18, 19]. Moreover, PLAL has numerous advantages compared to other nanoparticle production methods [13]. It leads to successful production of colloidal, pure and contamination-free nanoparticles [20, 21]. Our group previously showed that PLAL is a suitable method for the production of InN-NCs with hexagonal crystalline structure. Colloidal InN-NCs were produced in ethanol by ablating the HPCVD-grown InN thin film sample with different energies using a nanosecond pulsed laser. The average diameter of the produced InN-NCs was 10 nm [18]. These InN-NCs were shown to have applications such as a near infrared range photodetector [22] and charge trapping memory cells [23]. However, the starting material was HPCVD-grown InN thin film and the starting material, either a bulk target or a suspension, affects the final nanoparticle size in PLAL. It was previously shown that pulsed laser ablation of suspensions results in much smaller nanoparticle sizes compared to the ablation of bulk target. It was suggested that the particles in the suspension absorb all the laser energy since the particles encounter multiple pulses during all the ablation process due to continuous stirring. On the other hand, the laser energy is absorbed only by the target in case of ablation of bulk target and results in larger nanoparticles. Furthermore, the particle size of the nanoparticles at the end of the ablation process depends on the initial size of the suspended particles [24, 25].

In this study, we aimed to produce ultra-small InN-NCs by using suspension of micron-sized InN powder in ethanol with PLAL method and, to our knowledge, we reached the smallest nanocrystal size for InN-NCs in the literature. For this purpose, we performed series of PLAL processes with different solvents (isopropanol, ethanol and water), different laser energies (3, 4 and 5 mJ) and different ablation times (up to 300 min). The formation of InN-NCs was confirmed by using scanning electron microscope (SEM) and transmission electron microscope (TEM). Moreover, we used X-ray diffraction (XRD) to confirm the crystal structure of InN-NCs. Absorption, zeta potential and RAMAN analyses were performed for further characterization of the nanocrystals. We showed that formation mechanism of InN-NCs was through pulsed laser fragmentation and melting by analyzing the SEM. We successfully demonstrated the presence of fragmented/molten particles and nanoparticles in the SEM images. Moreover, the hexagonal crystalline structure of the powder target was preserved after the nanoparticle formation. Overall, we proposed a roadmap for the generation of ultra-small (<5 nm) InN-NCs by combination of PLAL and suspension of micron-sized target after optimizing the laser parameters such as liquid environment, laser ablation time, laser energy and applying centrifugation with appropriate time and speed as a post-synthesis treatment.

2 Experimental

2.1 Nanocrystal synthesis

InN-NCs were generated by using a commercial nanosecond pulsed ND:YLF laser (Empower Q-Switched Laser, Spectra Physics) operating at 527 nm with a 100 ns pulse duration and 1 kHz repetition rate. InN target was purchased as powder (Santa Cruz Biotechnology, USA) and 1 mg powder was dissolved in 10 ml of pure solvent (isopropanol, ethanol and water). To obtain a well dispersed InN-NC solution, the colloidal nanomaterial solution was continuously stirred by a magnetic stirrer at 1000 rpm during the laser ablation process. The colloidal solution was light orange after nanoparticle formation for all experiments. In all laser ablation procedures, the laser beam was focused on InN solution by the help of a plano-convex lens with a focal length of 50 mm. The laser power for the ablation process varied in different processes as 3, 4 and 5 W with corresponding pulse energies of 3, 4 and 5 mJ, respectively. As another parameter to test, different ablation durations starting from 1 to 300 min were studied. 15 min of centrifugation at 4000×*g* was also performed for two samples obtained with 3 mJ pulse energy (15 and 60 min ablation time) to make the nanocrystals smaller than 5 nm isolated in HR-TEM images.

2.2 Nanocrystal characterization

Different characterization methods were utilized throughout this study. The high-resolution transmission electron microscope (HR-TEM) imaging of the InN-NCs was carried out by using the FEI-Tecnai G^2 F30 TEM instrument at an operating voltage of 300 kV. All samples were prepared by drop-casting the solutions onto separate carbon-coated TEM grids. Each histogram data were obtained by counting 100 particles from the TEM images and using Image J Image Processing and Analysis software. The morphology and the time course of the nanoparticle generation were monitored by using scanning electron microscope (SEM, Quanta 200 FEG, FEI Instruments, USA). For the stability analyses, zeta potential measurement was carried out (Malvern Instruments Ltd, Malvern, UK). Absorption analysis of the InN-NCs was performed in 200–800 nm range (Varian Cary 100 UV/Vis spectrophotometer). To determine the crystalline structure and the composition of the InN-NCs, X-ray diffraction (XRD) analysis was performed (PANalytical X'Pert PRO multipurpose diffractometer, Netherlands). The operation voltage was 45 kV and the current was 40 mA with a CuKα radiation source. The sample was prepared by depositing and drop-casting the InN-NCs on quartz substrate. Raman spectroscopy was performed by using a Witec Alpha 300 S Micro Raman spectrometer with a Nd:YAG laser at an excitation wavelength of 532 nm (laser power: 10 mW, laser spot size ~4 μm, unpolarized) and a Nikon 100x (N.A. = 0.9) air objective. The integration time was 1.035 s and we obtained the data in 3.5 h. The sample was dropcasted onto a Si substrate with <111> orientation.

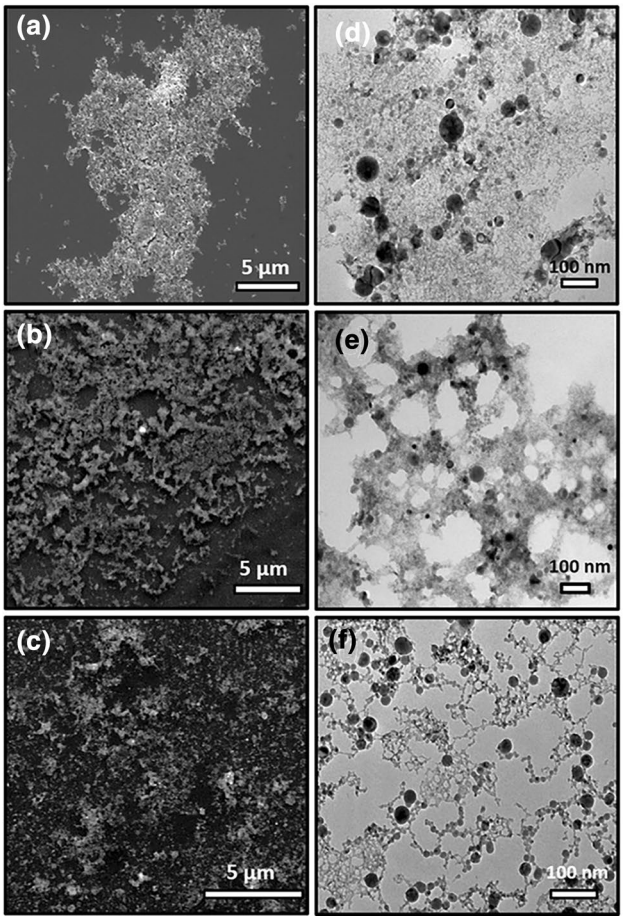

Fig. 1 SEM and TEM images of InN-NCs produced in **a, d** ethanol, (**b**, the sample was dropcasted onto) isopropanol and **c, f** water. InN-NCs smaller than 50 nm were successfully produced in all of three solvents

3 Results and discussion

3.1 Stability issue of InN-NCs in different solvents

Stability of the produced nanoparticles is a challenging issue and PLAL has the advantage of production of stable nanoparticles even without using any stabilizers or surfactants [26]. It was shown that the solvent plays a significant role in the stability of produced nanoparticles with PLAL [27]. Thus, we first aimed to determine the most appropriate solvent in which InN-NCs is stable. For this purpose, we used ethanol, isopropanol and distilled water and performed laser ablation for 30 min at 3 mJ laser energy. SEM (Fig. 1a–c) and TEM (Fig. 1d–f) images showed that InN-NCs smaller than 50 nm were successfully produced in all of three solvents and no aggregation was observed in freshly synthesized samples.

On the other hand, zeta potential measurement of these samples (Fig. 2) demonstrated that InN-NCs

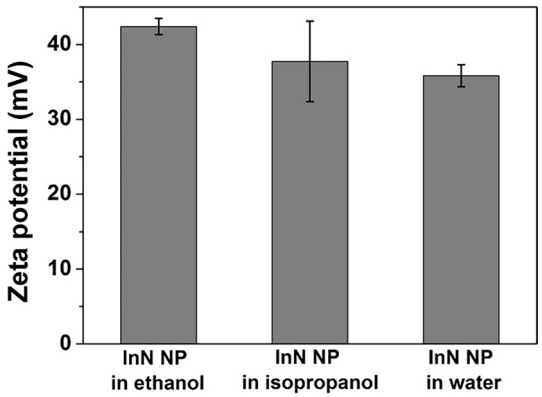

Fig. 2 Zeta potential graph for InN-NCs produced in ethanol, isopropanol and water. Zeta potential values were 42.40 ± 1.08, 37.73 ± 5.38 and 35.83 ± 1.48 mV for the InN-NCs produced in ethanol, isopropanol and water, respectively. The most stable InN-NCs were produced in ethanol

produced in ethanol has the highest zeta potential value (42.40 ± 1.08 mV) compared to the InN-NCs in isopropanol and water (37.73 ± 5.38 and 35.83 ± 1.48 mV, respectively). Thus, ethanol was determined as the most appropriate solvent for InN-NCs to be produced in terms of stability.

3.2 Effects of laser energy and ablation duration on InN-NCs

Laser energy was shown to be a significant parameter for nanoparticle production with PLAL method, specifically for the size distribution of the nanoparticles [28]. Hence, we focused on the effect of laser energy on the InN-NC particle size. 3, 4 and 5 mJ laser energies were investigated in 60 min ablation duration. TEM images were obtained for InN-NCs produced with each laser energy (Fig. 3 a–c) and the average diameter of InN-NCs was calculated using the histogram data (Fig. 3 d–f). The smallest mean size of the InN-NCs was observed in ablation with 3 mJ laser energy (10.84 ± 0.71 nm) while ablation with 4 and 5 mJ resulted in 16.27 ± 0.68 and 16.06 ± 0.59 nm, respectively. Thus, smaller InN-NCs were obtained by using lower laser energy in ablation procedure. In a previous study, we showed that the lower pulse energies with nanosecond laser ablation of InN thin film led to a decrease in the nanoparticle size distribution but the smaller nanoparticles were obtained with larger energies [22]. The target material has a great importance since the laser pulse with higher energy result

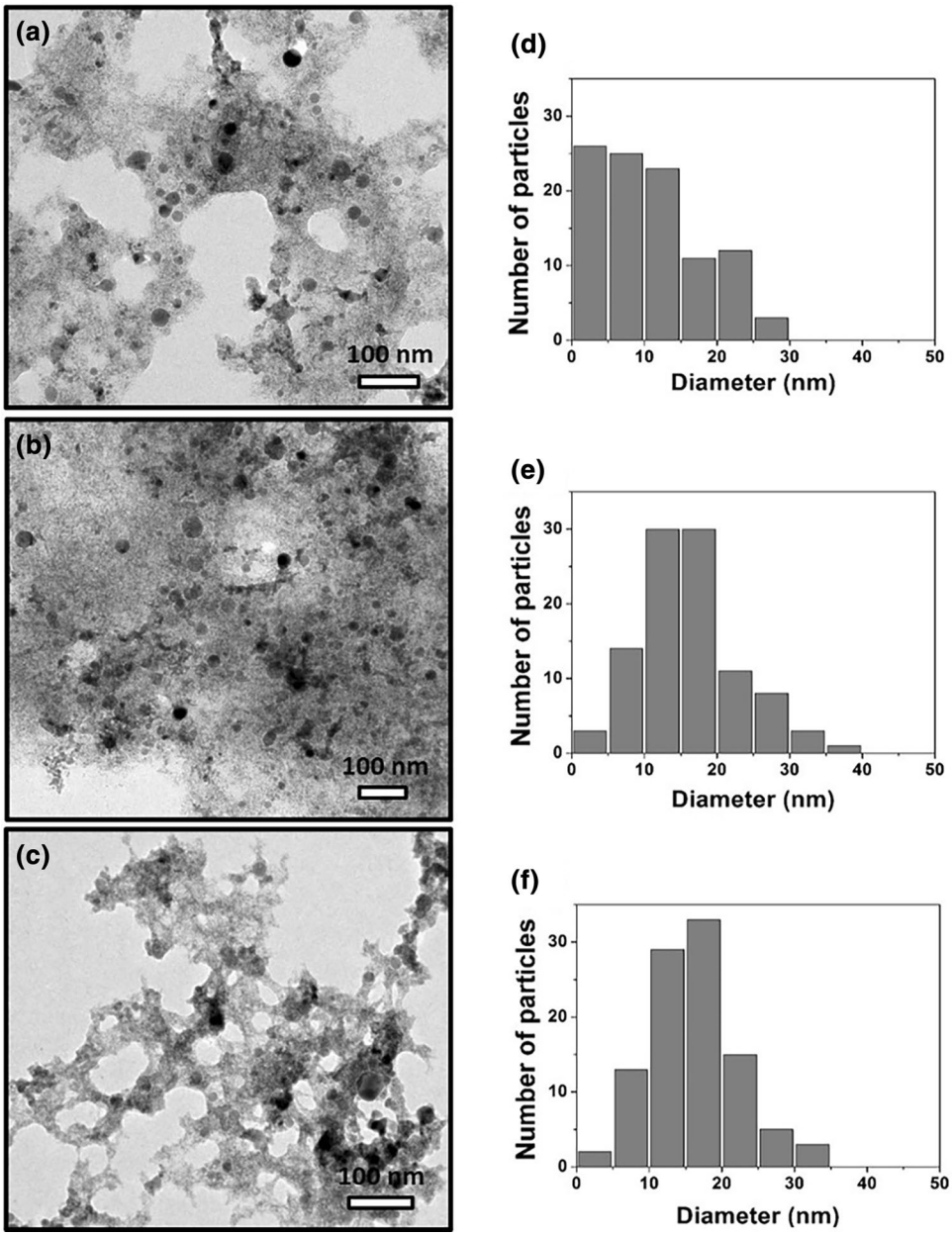

Fig. 3 TEM images and histogram data of InN-NCs produced with **a, d** 3 mJ, **b, e** 4 mJ and **c, f** 5 mJ laser energies. The average InN-NC diameters were determined as 10.84 ± 0.71, 16.27 ± 0.68 and 16.06 ± 0.59 nm for the laser energies of 3, 4 and 5 mJ, respectively. 3 mJ laser energy resulted in the smallest nanoparticle diameter and narrower size distribution

in much more ablation process on the solid target while the increase in the energy did not affect the nanoparticle sizes after a certain value with the continuously stirred sample powder sample.

It was demonstrated that nanoparticles start to aggregate and precipitate when the ablation duration increases [29]. Therefore, we used different laser ablation durations at 3 mJ laser energy to optimize the ablation duration and to observe the formation mechanism of InN-NCs. SEM images were analyzed in terms of ablation durations (5, 15, 30, 60, 90, 120, 180 min) (Fig. 4 b–h) starting from the InN powder samples consisting of micron-sized InN flakes (Fig. 4a). When the laser interacted with the InN powder, it caused melting in the interacted area. On the other hand, increased temperature in the non-interacted area resulted in formation of nanoparticles and molten particles on the powder surface as shown in the inset of Fig. 4b. Nanoparticle production began at 15-min ablation duration. The SEM image of 15-min ablated sample clearly showed that there were also fragmented particles together with molten spherical particles. Furthermore, with increasing ablation durations, firstly micron particles (powder, fragmented, molten particles) disappeared and nanoparticles seemed to be decreasing in size. However, the decrease in size led to aggregation after 60-min ablation.

After a topographical analysis with SEM, TEM images were obtained to evaluate the size distribution of the InN-NCs. As depicted in TEM images (Fig. 5a–d), we obtained smaller nanoparticles with a narrower size distribution with increasing ablation duration. This was also confirmed with the aforementioned SEM analysis. However, after 15-min ablation, the size distribution got broader and the mean size of the InN-NCs increased. This might be because of the fact that the smaller the nanoparticles, the more aggregation is observed. The micron-sized particles were not included in the histogram analysis for the 15-min ablation process.

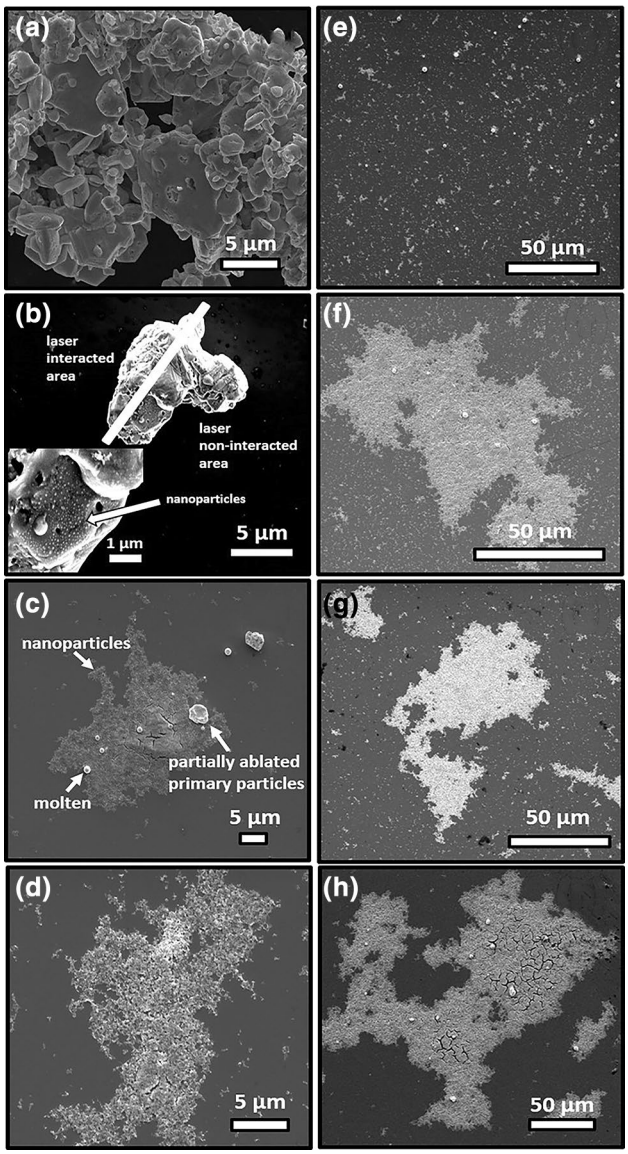

Fig. 4 SEM images of InN **a** powder, and nanoparticles after **b** 5 min, **c** 15 min, **d** 30 min, **e** 60 min, **f** 90 min, **g** 120 min and **h** 180 min ablation durations

3.3 Post-synthesis treatment

One of the interesting properties of InN-NCs is the optical behavior of nanoparticles produced with different ablation times that lead to different particle sizes. To analyze the optical properties of InN-NCs, we further determined the absorption behavior in UV–Vis spectra from 200 to 800 nm (Fig. 6). InN-NCs demonstrated an increased absorption intensity in two main UV regions (200 and 300 nm) after 15-min ablation time. When the ablation duration increased, the intensity in the spectra increased since the concentration of the nanoparticles increased. On the other hand, the shoulder of the peak in the 300-nm region became more pronounced after 60-min ablation due to the aggregation of the nanoparticles. This aggregation led to larger nanoparticle size and a red shift in the UV–Vis spectra. We further analyzed the optical behavior of nanoparticles up to 300 min and observed that there was no significant change on the optical behavior providing the stable particle sizes.

Although we were able to obtain the histogram data, much smaller nanoparticles distinguished by TEM images (Fig. 5) might not be easily detected in UV–Vis spectra due to the larger nanoparticles. To determine the size and behavior of these smaller nanoparticles, we used centrifugation technique. For this purpose, we focused on two different ablation durations, 15 and 60 min. After the centrifugation process, we checked the absorption behavior of the nanoparticles (Fig. 7a, b). When compared to the samples before centrifugation, the spectra shifted to UV

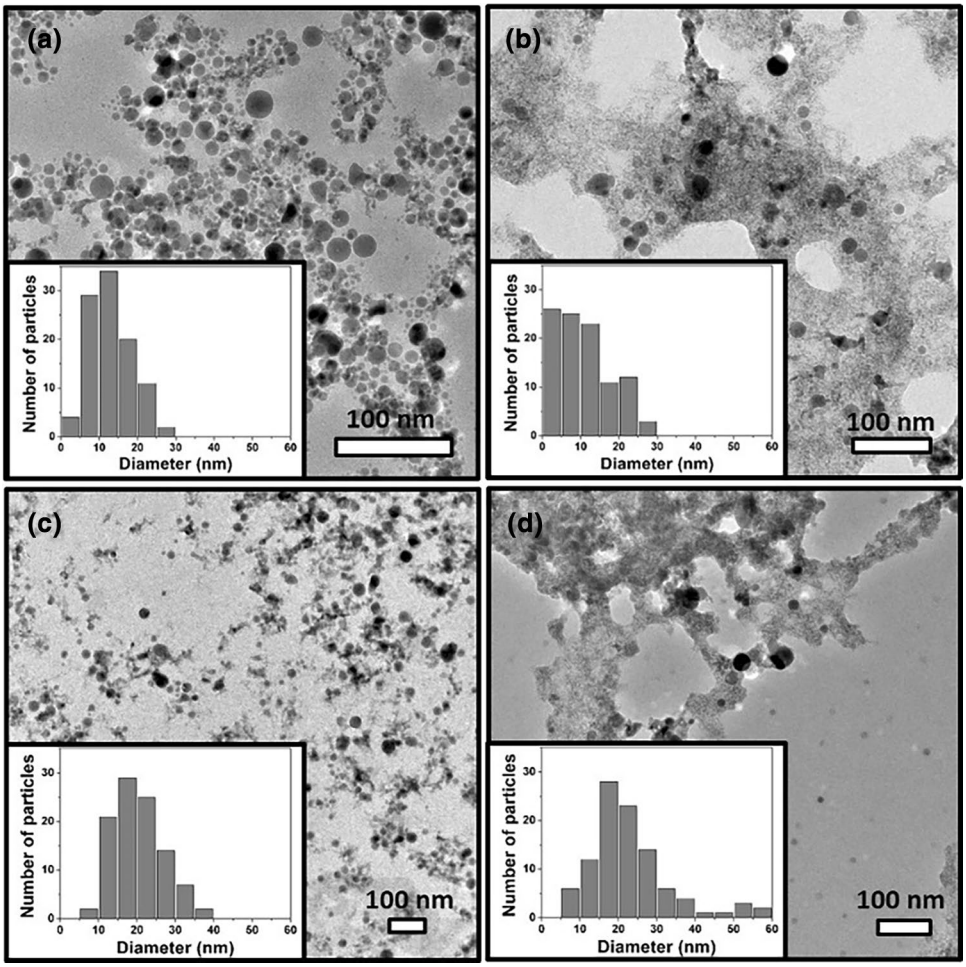

Fig. 5 TEM images of InN-NCs at **a** 15 min, **b** 60 min, **c** 120 min, **d** 180 min laser ablation durations. As the ablation duration increases, the size distribution of the InN-NCs increases

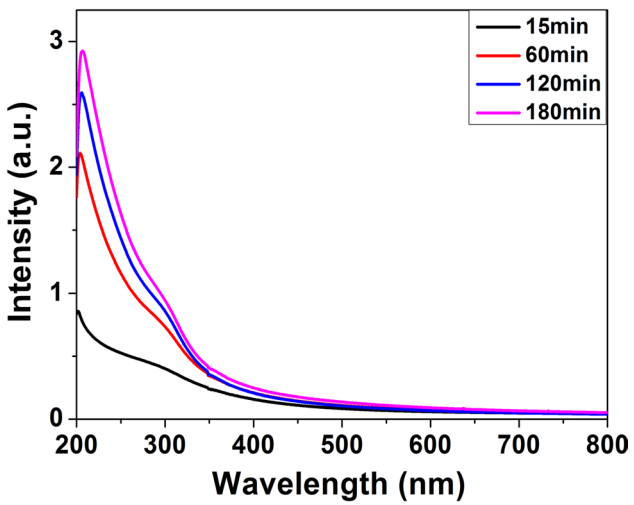

Fig. 6 Absorption of InN-NCs produced at different ablation durations. The intensity throughout the UV region increases with increasing ablation duration. Moreover, the aggregation of InN-NCs after a certain ablation duration, namely 60 min, leads to a shoulder with a red shift in the peak at around 300 nm

region demonstrating that centrifugation process was successful in selecting the smaller nanoparticles. The intensity also decreased for the InN-NCs produced at 60-min laser ablation duration, which might be due to the unoptimized centrifugation process. However, zeta potential analysis (Fig. 7c) revealed that when the samples were centrifuged, stability was conceded since the zeta potential values decreased after centrifugation. The decrease in the stability is consistent with the previous data indicating that smaller nanoparticles have the tendency of faster aggregation [30]. Moreover, as discussed previously, the centrifugation of 60-min ablated sample resulted in a higher zeta potential value when compared to that of the 15-min ablated and centrifuged sample. This is also consistent with the size analysis since 15-min ablation led to much smaller InN-NC sizes and a faster aggregation as inferred from the zeta potential values. To obtain a more stable colloidal nanoparticle solution produced by PLAL, it was suggested in some previous studies that surfactants and stabilizers can be used [31, 32]. TEM and HR-TEM images were obtained for 15- and 60-min ablated samples (Fig. 8). TEM data showed that after centrifugation, much smaller InN-NCs,

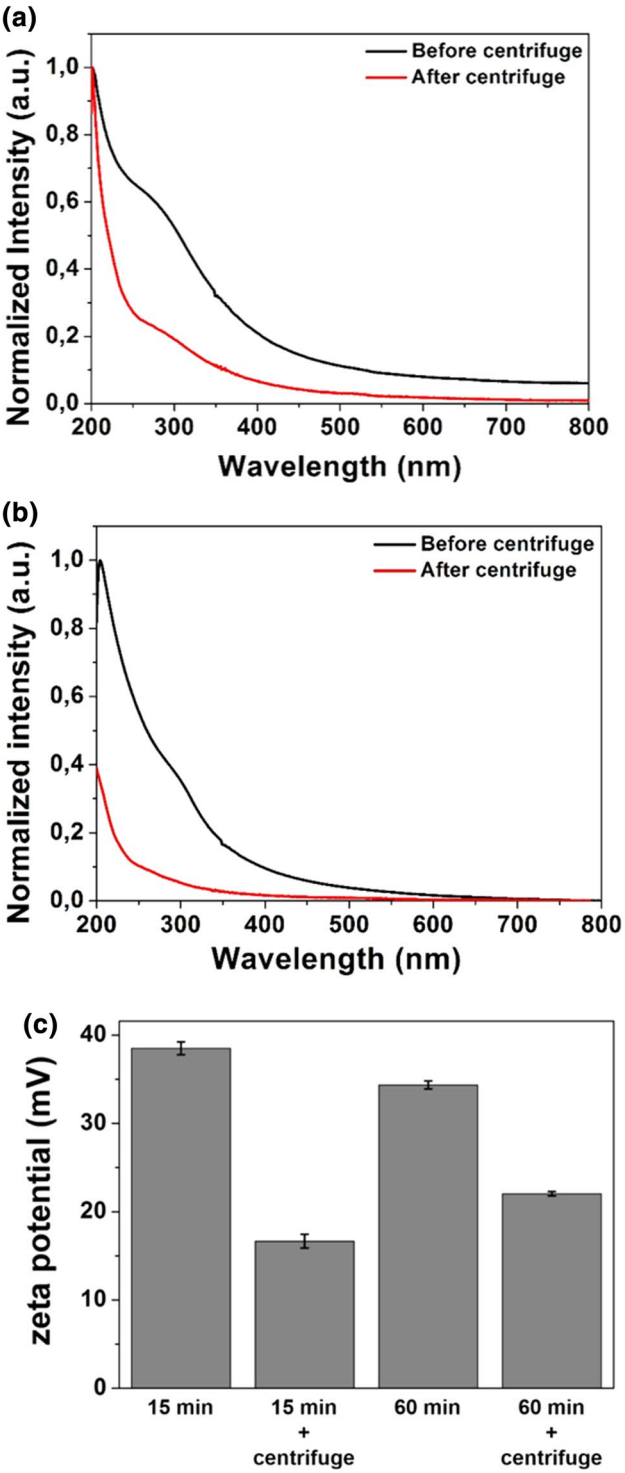

Fig. 7 Absorption of InN-NCs produced at **a** 15 min and **b** 60 min ▶ ablation duration before and after centrifugation. Centrifugation process results in the elimination of the larger nanoparticles in the colloidal suspension, thus leading to the disappearance of the peak around 300 nm wavelength. Smaller nanoparticles display the absorption through the UV region. **c** The zeta potential values of InN-NCs produced at 15 and 60 min ablation duration before and after centrifugation. The zeta potential of InN-NCs produced at 15 and 60 min ablation duration are 38.5 ± 0.72 and 34.36 ± 0.46 mV, respectively. However, after centrifugation the zeta potential values decreased to 16.66 ± 0.79 and 22.03 ± 0.24 mV for the nanoparticles produced at 15 and 60 min ablation duration, respectively

which were previously observed as a background, became noticeable due to the disappearance of larger nanoparticles. Moreover, it was demonstrated with HR-TEM analysis that the InN-NCs had crystalline structure. Both single-crystalline and polycrystalline InN-NCs were observed in TEM analysis. The HR-TEM image of the single-crystalline InN-NC in the inset of Fig. 8c reveals the crystalline lattice fringes having a lattice spacing of 0.28 nm, corresponding to (002) plane of hexagonal InN-NC [17, 18, 33]. TEM images from centrifuged samples allowed us to determine the size of nanoparticles smaller than 5 nm. The histogram analysis (Fig. 9) showed that we obtained InN-NC smaller than 5 nm in both 15- and 60-min ablated samples.

3.4 Crystal structure analysis

After the InN-NCs were confirmed to be in crystalline form from the HR-TEM images, we studied the crystal structure in detail by using XRD. XRD analysis results of the powder target, 15 and 60 min ablated samples are shown in Fig. 10. The peaks of 15 and 60 min ablated samples at two theta degrees of 28.92, 31.14, 32.96, 36.10, 43.13, 51.46 and 56.82 indicated that InN-NCs had hexagonal crystal structure. Moreover, there were In_2O_3 diffraction peaks at two theta degrees of 30.38, 32.72, 35.22, 38.93, 54.23 as shown in the figure. Since we used ethanol as the solvent, In_2O_3 was generated in the solution as a byproduct, together with In metal which had a quite small peak at two theta degrees of 36.10. In_2O_3 peaks became more intense in the sample ablated for 60 min indicating that increased ablation times resulted in more oxidation of the nanoparticles. The same hexagonal InN peaks also appeared in the XRD analysis of the target powder confirming that the process included pulsed laser fragmentation, thus the crystalline phase of the nanoparticles did not change during the production process. Moreover, the molten nanoparticles observed in SEM images do not seem to be modified in terms of crystal structure, which shows that melting did not have any effect on the crystallinity of InN-NCs. The XRD peaks are in a good agreement with the XRD data presented in the literature for the InN-NCs produced or grown with different techniques [6, 10, 11]. Furthermore, In metal and In_2O_3 peaks, except for the one at the 2 theta degree of 30.38, were also present in the XRD analysis of InN powder suggesting that a purer starting material consisting of only InN would result in a colloidal InN-NC solution with less In_2O_3.

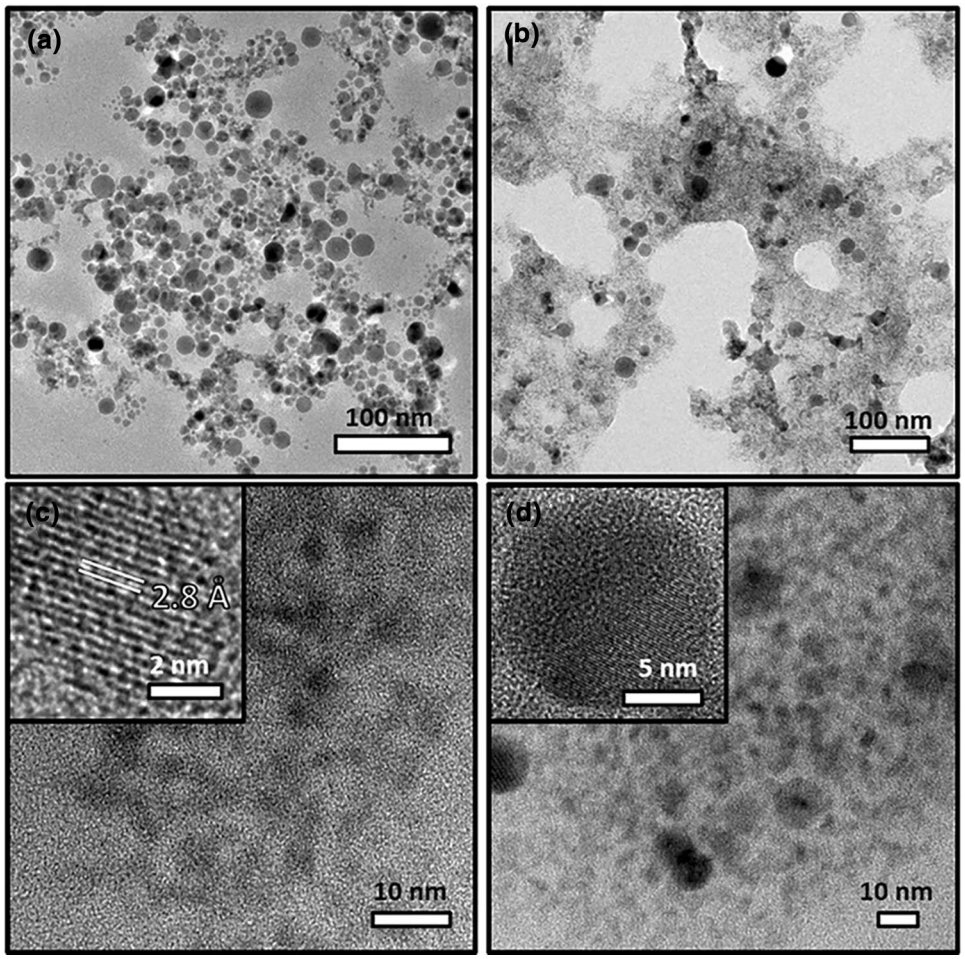

Fig. 8 TEM images of InN-NCs produced at **a** 15 min and **b** 60 min laser ablation durations. To determine the size of InN-NCs smaller than 5 nm, a centrifugation process was performed and TEM images of the centrifuged samples of **c** 15 min and **d** 60 min ablated InN-NCs are represented. The *inset images* demonstrate the crystalline structure of InN-NCs. The 0.28 nm lattice fringe confirms the (002) plane of hexagonal InN-NC

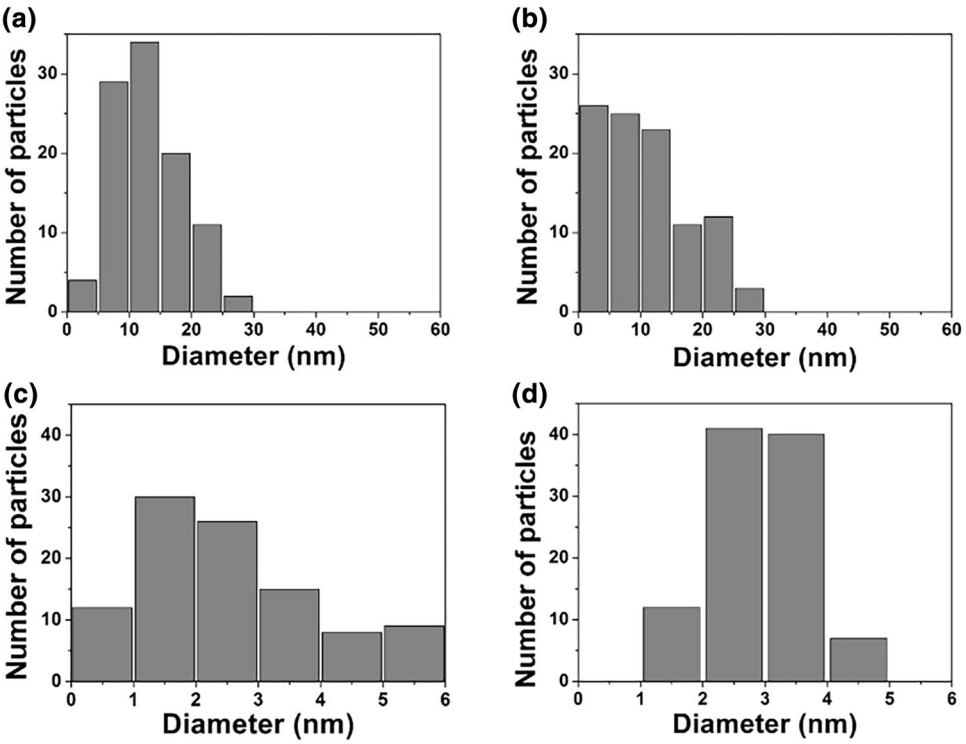

Fig. 9 Histogram of InN-NCs produced at **a** 15 min and **b** 60 min. After centrifugation of **c** 15 min and **d** 60 min ablated InN-NCs, the ones smaller than 5 nm could be determined

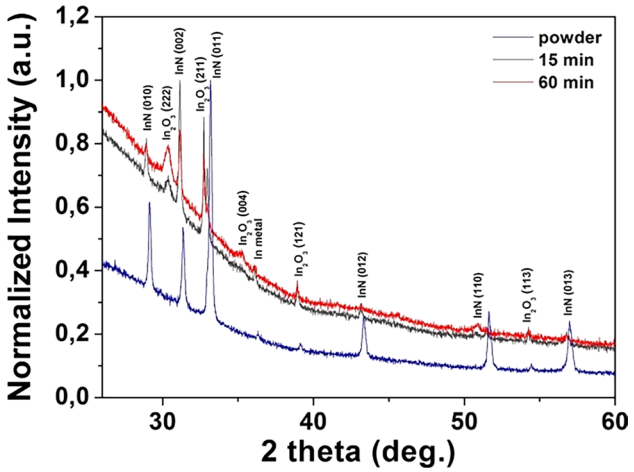

Fig. 10 XRD analysis of InN powder as the starting material and InN-NCs after 15 and 60 min laser ablation process. InN powder was shown to be consisting of hexagonal InN together with In metal and In_2O_3. After 15 and 60 min laser ablation, the hexagonal phase of the nanoparticles did not differ from the phase of the InN powder, which indicated the formation mechanism was through fragmentation. Moreover, the intensity of In_2O_3 peaks increase in 60-min ablated samples when compared to the 15-min samples, implying that longer ablation durations lead to more oxidation of the sample

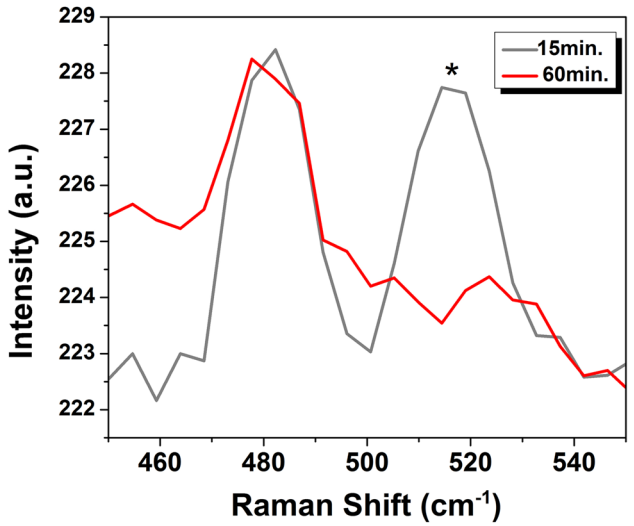

Fig. 11 RAMAN spectra of InN-NCs produced at 15 and 60 min. Sharp peaks at 481.68 and 479.85 cm^{-1} correspond to E_2 mode of the hexagonal InN-NCs. The peak at 516.46 cm^{-1} shows the RAMAN spectrum of Si substrate, which has a <111> orientation

3.5 RAMAN investigation

Another characterization method for InN-NCs is the Raman spectroscopy analysis. 15 and 60 min ablated samples were analyzed and it was found that the sharp peaks at 481.68 and 479.85 cm^{-1}, respectively, correspond to E_2 mode of the hexagonal InN-NCs (Fig. 11). The InN-NC RAMAN peaks and XRD data confirmed the hexagonal phase of the InN-NCs, which is also consistent with the literature [6, 12]. The peak at 516.46 cm^{-1} shows the RAMAN spectrum of Si substrate.

4 Conclusions

In this study, we showed for the first time that ultra-small InN-NCs (<5 nm in diameter) can be produced from InN powder target by using PLAL technique. We demonstrated that lower laser energy and lower ablation duration result in much smaller nanoparticles since even if the ablation time increased and the smaller nanoparticles were produced, they tended to aggregate. Hexagonal InN-NCs smaller than 5 nm in diameter were produced in ethanol with optimized ablation conditions successfully. We showed that PLAL is a suitable technique for production of InN-NCs, which is a Group III nitride. Thus, other nitrides in the same group might be successfully produced with this technique. As an outlook of InN-NC production with PLAL method, ablation with femtosecond laser pulses might be studied to overcome the low decomposition temperature disadvantage of InN material.

Acknowledgements This research was partially supported by TÜBA-GEBİP. We thank Hüseyin Avni Vural for his assistance with RAMAN investigation. We would also like to show our gratitude to Dr. Tolga Bağcı for reading and making comments that improved the manuscript.

References

1. B. Monemar, J. Mater. Sci. Mater. Electron. **10**, 227 (1999)
2. A.G. Bhuiyan, A. Hashimoto, A. Yamamoto, J. Appl. Phys **94**, 2779 (2003)
3. I. Mahboob, T.D. Veal, C.F. McConville, H. Lu, W.J. Schaff, Phys. Rev. Lett. **92**, 36804 (2004)
4. S.K. O'Leary, B.E. Foutz, M.S. Shur, L.F. Eastman, Appl. Phys. Lett. **88**, 152113 (2006)
5. X. Michalet, S.S. Gambhir, S. Weiss, Science **307**, 538 (2005)
6. M.S. Hu, W.M. Wang, T.T. Chen, L.S. Hong, C.W. Chen, C.C. Chen, Y.F. Chen, K.H. Chen, L.C. Chen, Adv. Funct. Mater **16**, 537 (2006)
7. O. Briot, B. Maleyre, and S. Ruffenach. Appl. Phys. Lett. **83**, 2919 (2003)
8. N. Nepal, N.A. Mahadik, L.O. Nyakiti, S.B. Qadri, M.J. Mehl, J.K. Hite, C.R. Eddy, Cryst. Growth Des. **13**, 1485 (2013)
9. A.P. Lima, A. Tabata, J.R. Leite, S. Kaiser, D. Schikora, B. Schöttker, T. Frey, D.J. As, K. Lischka, J. Cryst. Growth **201**, 396 (1999)
10. J.C. Hsieh, D.S. Yun, E. Hu, A.M. Belcher, J. Mater. Chem. **20**, 1435 (2010)
11. A. K. Mann, D. Varandani, B. R. A. J. Mehta, Bull. Mater. Sci. **31**, 233 (2008)
12. J. Xiao, Y. Xie, R. Tang, W. Luo, Inorg. Chem. **42**, 107 (2003)
13. S. Hu, Y. Dong, J. Yang, J. Liu, S. Cao, J. Mater. Chem. **22**, 1957 (2012)

14. M.A. Qaeed, K. Ibrahim, K.M.A. Saron, A. Salhin, Sol. Energy **97**, 614 (2013)
15. P. Šimek, D. Sedmidubský, K. Klímová, Š. Huber, P. Brázda, M. Mikulics, O. Jankovský, Z. Sofer, J. Nanopart. Res. **16**, 2805 (2014)
16. K. Sardar, F.L. Deepak, A. Govindaraj, M.M. Seikh, C.N.R. Rao, Small **1**, 91 (2005)
17. C. Wu, T. Li, L. Lei, S. Hu, Y. Liu, Y. Xie, M. Eng. New J. Chem. **29**, 1610 (2005)
18. S. Alkis, M. Alevli, S. Burzhuev, H.A. Vural, A.K. Okyay, B. Ortaç, J. Nanopart. Res. **14**, 1048 (2012)
19. T. Oztas, H.S. Sen, E. Durgun, B. Ortaç, J. Phys. Chem. C **118**, 30120 (2014)
20. F. Lin, J. Yang, S.-H. Lu, K.-Y. Niu, Y. Liu, J. Sun, X.-W. Du, J. Mater. Chem **20**, 1103 (2010)
21. S. Hu, Y. Guo, Y. Dong, J. Yang, J. Liu, S. Cao, J. Mater. Chem **22**, 12053 (2012)
22. B. Tekcan, S. Alkis, M. Alevli, N. Dietz, B. Ortac, N. Biyikli, A. K. Okyay, IEEE Electron Device Lett. **35**, 936 (2014)
23. N. El-Atab, F. Cimen, S. Alkis, B. Ortaç, M. Alevli, N. Dietz, A.K. Okyay, A. Nayfeh, Appl. Phys. Lett. **104**, 253106 (2014)
24. D. Kim, D. Jang, Appl. Surf. Sci **253**, 8045 (2007)
25. H. Zeng, X.W. Du, S.C. Singh, S.A. Kulinich, S. Yang, J. He, W. Cai, Adv. Funct. Mater **22**, 1333 (2012)
26. V. Amendola, M. Meneghetti, Phys. Chem. Chem. Phys. **11**, 3805 (2009)
27. R. M. Tilaki, a. Iraji zad, and S. M. Mahdavi, Appl. Phys. A **84**, 215 (2006).
28. A. Hahn, J. Laser Micro/Nanoeng. **3**, 73 (2008)
29. A. Schwenke, P. Wagener, S. Nolte, S. Barcikowski, Appl. Phys. A Mater. Sci. Process **104**, 77 (2011)
30. H. Zhang, R.L. Penn, R.J. Hamers, J.F. Banfield, J. Phys. Chem. B **103**, 4656 (1999)
31. F. Mafune, J. Kohno, Y. Takeda, T. Kondow, H. Sawabe, J. Phys. Chem. B **104**, 9111 (2000)
32. F. Mafuné, J. Kohno, Y. Takeda, J. Phys. Chem. B **105**, 5114 (2001)
33. M. Lei, K. Huang, R. Zhang, H.J. Yang, X.L. Fu, Y.G. Wang, W.H. Tang, J. Alloys Compd. **535**, 50 (2012)